Water Droplet Bouncing and Superhydrophobicity Induced by Multiscale Hierarchical Nanostructures

Doo Jin Lee,[†] Hyung Min Kim,[†] Young Seok Song,[‡,*] and Jae Ryoun Youn[†,*]

[†]Research Institute of Advanced Materials (RIAM), Department of Materials Science and Engineering, Seoul National University, Daehak-Dong, Gwanak-Gu, Seoul 151-744, Korea and [‡]Department of Fiber System Engineering, Dankook University, 126 Jukjeon-dong, Suji-gu, Yongin-si, Gyeonggi-do 448-701, Korea

ABSTRACT

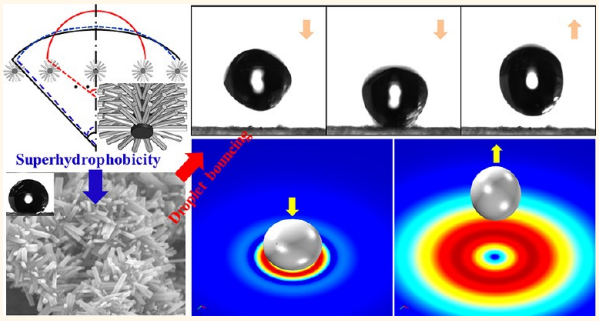

Superhydrophobicity of multiscale hierarchical structures and bouncing phenomenon of a water droplet on the superhydrophobic surface were studied. The multiscale hierarchical structures of carbon nanotube/ZnO and ZnO/carbon nanofiber were produced by the hydrothermal method. The multiscale hierarchical structure showed superhydrophobicity with a static contact angle (CA) larger than 160° due to increased air pockets in the Cassie–Baxter state. The water bouncing effect observed on the multiscale hierarchical nanostructure was explained by the free energy barrier (FEB) analysis and finite element simulation. The multiscale hierarchical nanostructure showed low FEBs which provoke high CA and bouncing phenomenon due to small energy dissipation toward receding and advancing directions.

KEYWORDS: superhydrophobicity · water bouncing · hierarchical nanostructures · thermodynamical analysis · droplet deformation

Superhydrophobicity is a distinctive characteristic of surface structure implying extreme water repellency and a contact angle (CA) over 150°. Many researchers have produced biomimetic superhydrophobic surfaces with extremely high water repellency for industrial applications such as self-cleaning windows, windshield, exterior paints, antifouling, roof tiles, and textiles.

One of the simplest ways for introducing superhydrophobicity is to create geometries with vertically aligned pillar textures on a surface, which offers plenty of air pockets between the pillars and maintains the so-called Cassie–Baxter state.[1] Various attempts have been made using nanostructures, such as carbon nanotubes (CNTs) and nanopins. For instance, vertically aligned CNT bundles (ACNT)[2] have shown superhydrophobicity with a CA of 158°, while PAN nanofiber bundles[3] and nanoneedle structures[4] that had much lower densities than ACNT have shown superior superhydrophobicity with CA values of 173° and 178°, respectively. Honeycomb like ACNT[5] with uniform geometry and a very low sliding angle of 3° has also been fabricated. Furthermore, other reports demonstrate that anisotropic dewetting tendency on the surface of a rice leaf can be imitated using the ACNT film and that anisotropic dewetting induced by different roll-off angles with respect to the rolling direction can be manipulated by the microstructural arrangement.[6]

Multiscale structures with microscale and nanoscale regularities, which are similar to downsized fractal structure of microscale structures (*e.g.*, lotus leaf, rose petal, feather, and butterfly wing), can provide superhydrophobicity by provoking larger CA, smaller contact angle hysteresis (CAH), smaller sliding angle, and a higher dynamic bouncing effect due to their structural characteristics. Sun *et al.* fabricated a multiscale structure of a biomimetic artificial leaf by nanocasting PDMS over the surface of a lotus leaf.[7] Indeed, many other dual-scale hierarchical structures mimicking the lotus leaf topography have been prepared using solvent-induced crystallization of typical polymers,[8] solvent etching,[9] anodization of fluorinated functional materials,[10] 3D microsphere/nanofiber networks,[11] self-assembly,[12,13] micropatterning of electrospun mats,[14] incorporation of

* Address correspondence to ysong@dankook.ac.kr, jaeryoun@snu.ac.kr.

Received for review March 12, 2012 and accepted August 28, 2012.

Published online August 28, 2012
10.1021/nn3032547

microbeads/nanobeads,[15,16] and nanostructures in a micro-ordered array.[17] The multiscale structures are full of air pockets due to their structural uniqueness. The air pockets in the hierarchical structure impede the transition from the Cassie–Bexter state to the Wenzel state and improve the morphological stability of a liquid droplet.[18] Consequently, the resulting multiscale roughness of the hierarchical structure yields extreme superhydrophobicity rather than the single-scale roughness.

From a theoretical perspective, the surface roughness morphology of multiscale nanostructures consisting of pillars with different height and width is desired not only to maximize CA but also to minimize the free energy barrier (FEB).[18–20] Furthermore, it makes the superhydrophobic state more stable and thus induces a larger self-cleaning effect, higher dynamic bouncing behavior, lower CAH, and smaller sliding angle. The dynamic bouncing effect may depend on the velocity of a dropping liquid, surface roughness morphology, and liquid properties. Compared with references related to the CA, a limited number of studies on the bouncing effect were reported. For example, Jung and Bhushan fabricated various surfaces including flat, nano-, micro-, and multiscale structures and proposed a criterion for determining the transition from the Cassie–Baxter regime to the Wenzel regime.[21,22] In addition, dimensionless numbers such as the Weber number (*We*), the Reynolds number (*Re*), and the Capillary number (*Ca*), have been used as a feasible determinant of whether the liquid droplet would show bouncing, sticking, or spreading behavior.[23]

In the current study, two kinds of multiscale structures were fabricated to investigate the superhydrophobicity and water bouncing phenomenon: (i) incorporation of 20 nm diameter CNT and 250 nm ZnO (CNT/ZnO), and (ii) combination of 20 nm diameter ZnO and 150 nm carbon nanofiber (ZnO/CNF). The prepared multiscale nanostructures[24] were modeled theoretically to predict the CA and CAH through the thermodynamic approach using surface free energy. The numerical results were compared with the experimental results. To the best of our knowledge, this is the first report that elucidates the underlying physics behind the bouncing phenomenon of a water droplet induced by the multiscale nanostructure with robust theoretical tools such as the free energy barrier (FEB) analysis and the level-set method.

RESULTS AND DISCUSSION

Hydrophobicity on the Various Structures. Many superhydrophobic surfaces in nature show hierarchical structures encompassing several micropattern and nanopattern levels arranged in a tree-like structure. When micropatterns are introduced onto a solid surface, a single-scale microroughness structure is generated due to the uniformity and regularity of the patterns, which contributes to a transition from the hydrophilic state to the hydrophobic one. When a solid–air interface exists due to air pockets under a liquid droplet, CA increases because the air pockets act as air cushions, and thereby the Cassie–Baxter regime[1] is generated. It should be noted that a liquid droplet in contact with a surface possessing microroughness may not be able to maintain the Cassie–Baxter state because the single-scale microroughness morphology is more susceptible to liquid intrusion than hierarchical structures.[18] Recent studies prove that hierarchical structures with multiscale roughness morphology have improved the liquid stability and superhydrophobicity.[18–20]

The present study has focused both on the hydrophobic nature of single-scale surface structures and on the dual-scale hierarchical structures that have been produced to introduce superhydrophobicity. For the single-scale surface structures, CNT forest, CNF forest, and ZnO pillars were explored, which had CA values of 120°, 120°, and 131°, respectively (see Figure 1). The high hydrophobicity of the CNT and CNF forests is associated with the nanoscale surface roughness of entangled CNTs and CNFs.[25] As well as the CNT forest, nanocomposites with CNTs protruding from the surface also showed high hydrophobicity, indicating that such CNT nanocomposites can offer hydrophobic surfaces by using a simple etching method (see Supporting Information, Figure 1). However, such forests and nanocomposites do not show superhydrophobicity due to their nonuniform surface roughness, low air–liquid-surface ratio, and thermodynamically unstable feature (*i.e.*, time-dependent transition from the Cassie–Baxter state to the Wenzel state[21]). Vertically aligned ZnO pillars have larger CA than either the CNT forest or the CNF forest since much space exists between the aligned ZnO pillars and the space forms air pockets supporting a liquid droplet resulting in highly hydrophobic nature of the surface.

To surpass the hydrophobicity limitation of the single-scale structure, hierarchical structures with a dual-scale of CNT/ZnO or ZnO/CNF were created, and the resulting hydrophobicity was investigated with a theoretical model. Hexagonal ZnO structures with a mean diameter of 20 nm have been fabricated on the CNF using the hydrothermal method. They created additional nanoscale surface roughness generating more air pockets, and subsequently a CA of 162° was obtained (Figure 2a,b). The hierarchical structures can lead to a hierarchical FEB structure, which results in the stable superhydrophobic state.[18] On the other hand, the CNT/ZnO hybrid structure has larger mean diameter (ZnO diameter of about 250 nm) than the ZnO/CNF structure (CNF diameter of about 150 nm) and yields a higher CA of 167.5° (*vs* 162°). In such a hierarchical structure, CNTs are networked with the ZnO pillars (Figure 2c,d). Many analytical approaches have been employed to predict the CA of superhydrophobic surfaces with single or multiscale roughness structures.[19–21,26] For

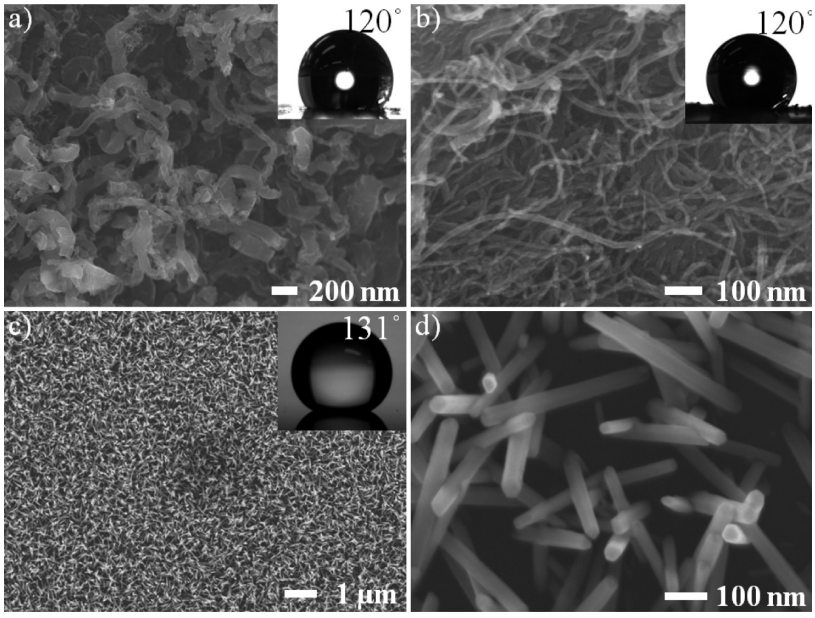

Figure 1. Single-scale surface morphology of (a) CNF forest, (b) CNT forest, (c) ZnO nanopillars, and (d) enlarged view of the ZnO nanopillars. Each system displays high hydrophobicity with the contact angle of 120°, 120°, and 131°, respectively.

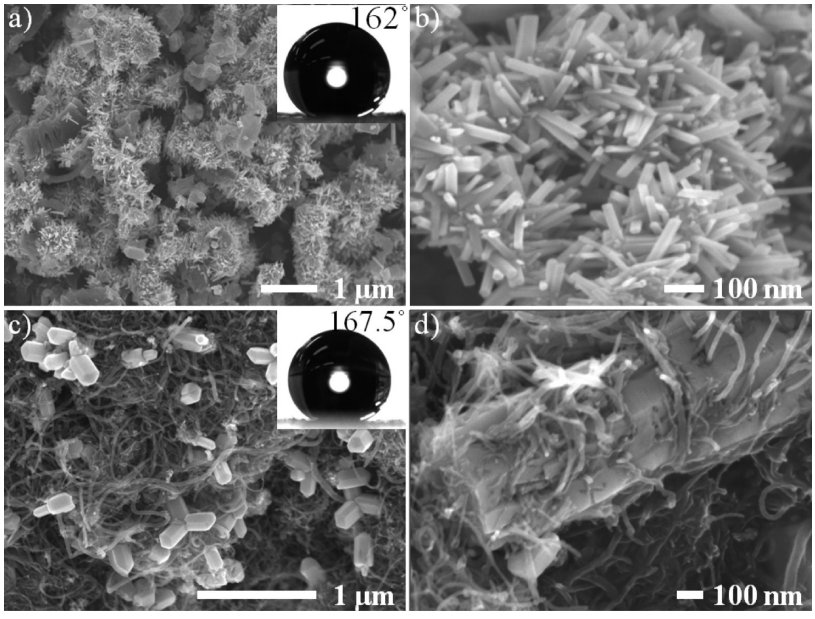

Figure 2. Multiscale hierarchical nanostructure: (a) ZnO/CNF hierarchical nanostructure showing superhydrophobicity with the contact angle of 162°, (b) enlarged view of the ZnO/CNF in which ZnO nanopillars are successfully grown onto the CNF, (c) CNT/ZnO hierarchical nanostructure showing higher superhydrophobicity with the contact angle of 167.5°, and (d) enlarged view of the CNT/ZnO in which CNTs are well networked with ZnO.

instance, the fractal formula can be used to analyze the CA of multiscale hierarchical structures[24] based on the fact that the hierarchical structures mimicking the lotus leaf have characteristics similar to that of the Koch curve in fractal geometry.

The multiscale hierarchical roughness structure fabricated in this study consisted of two different size pillars, micropillars and nanopillars, constructed on the base micropillars (Figure 3a). Thermodynamic analysis was carried out to explain the synergistic effect of the dual-scale roughness structures on CA. For the multiscale hierarchical system, the corresponding geometrical constitutions and free energy differences are expressed as below:[27]

$$\theta_i \frac{L_i^2}{\sin^2\theta_i} - (L_i^2 \cot\theta_i + (L_i + L_j)\cdot a \sin\theta_p) = \theta_j \frac{L_j^2}{\sin^2\theta_j} - L_j^2 \cot\theta_j \quad (1)$$

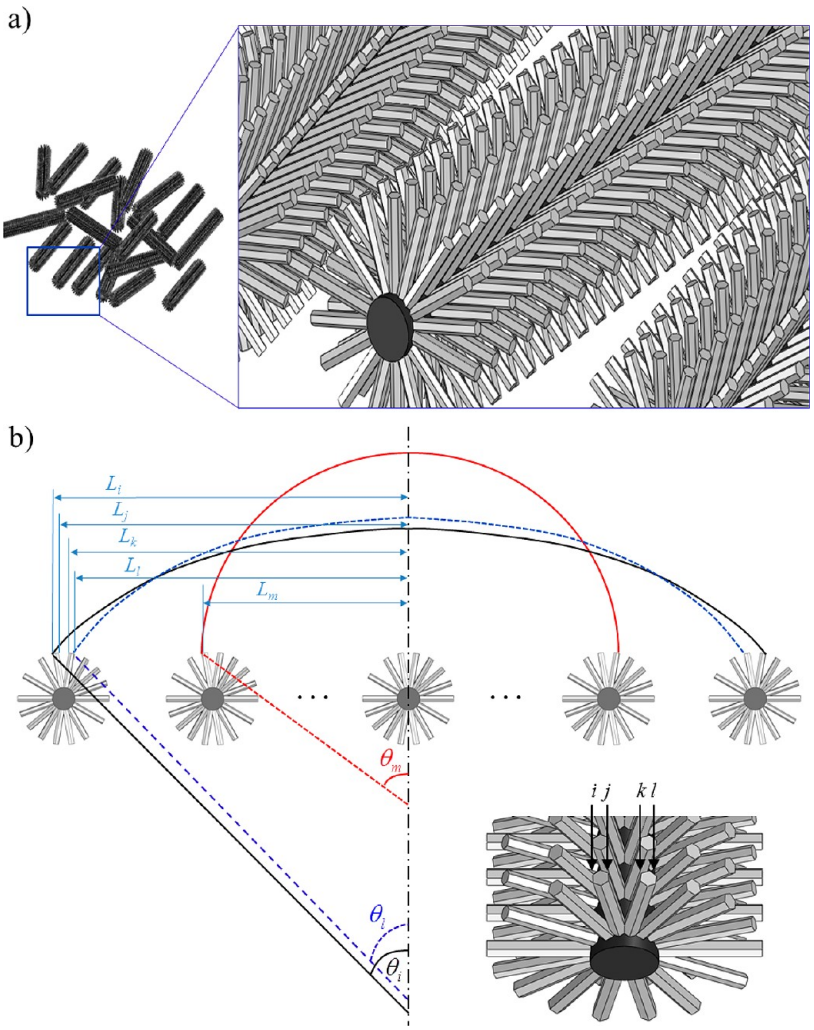

Figure 3. (a) Schematic illustration of the multiscale hierarchical system prepared in this study and (b) schematic cross-sectional configuration of a liquid droplet on the system.

$$\Delta F_{i\rightarrow j}/\gamma^{la} = \left(\theta_j \frac{L_j}{\sin\theta_j} - \theta_i \frac{L_i}{\sin\theta_i}\right) + a\cos\theta_Y \quad (2)$$

$$\theta_k \frac{L_k^2}{\sin^2\theta_k} - L_k^2\cot\theta_k = \theta_j \frac{L_j^2}{\sin^2\theta_j} - L_j^2\cot\theta_j \quad (3)$$

$$\Delta F_{j\rightarrow k}/\gamma^{la} = \left(\theta_j \frac{L_j}{\sin\theta_j} - \theta_k \frac{L_k}{\sin\theta_k}\right) + b \quad (4)$$

$$\theta_k \frac{L_k^2}{\sin^2\theta_k} - L_k^2\cot\theta_k + (L_k + L_l)\cdot a\sin\theta_p = \theta_l \frac{L_l^2}{\sin^2\theta_l} - L_l^2\cot\theta_l \quad (5)$$

$$\Delta F_{k\rightarrow l}/\gamma^{la} = \left(\theta_l \frac{L_l}{\sin\theta_l} - \theta_k \frac{L_k}{\sin\theta_k}\right) + a\cos\theta_Y \quad (6)$$

$$\theta_m \frac{L_m^2}{\sin^2\theta_m} - L_m^2\cot\theta_m = \theta_l \frac{L_l^2}{\sin^2\theta_l} - L_l^2\cot\theta_l \quad (7)$$

$$\Delta F_{l\rightarrow m}/\gamma^{la} = \left(\theta_l \frac{L_l}{\sin\theta_l} - \theta_m \frac{L_m}{\sin\theta_m}\right) + d \quad (8)$$

where θ_Y is Young's CA, θ_p is the angle between the two nanopillars, and the subscripts stand for the location of the droplet (Figure 3b). Here, *a*, *b*, and *d* are the width of the nanopillar, the interspacing between the nanopillars, and the interspacing between the micropillars, respectively. For a graphite sheet[28] and a flat ZnO film,[29] CAs are 98.3° and 100°, respectively. Equations 1, 3, 5, and 7 were derived by considering the geometrical constitution of the multiscale hierarchical nanostructure. When the edge of the meniscus of a water droplet moves from position *i* to *j*, the free energy (FE) difference is given by eq 2. The two FEs at each position characterized by surface tension and arc-length of the meniscus are $F_i = \gamma^{la}l_i^{la} + \gamma^{ls}l_i^{ls} + C$ and $F_j = \gamma^{la}l_j^{la} + \gamma^{sa}l_j^{sa} + C$, where *C* is the FE portion that remains unchanged during the calculation. The FE differences from position *j* to *k*, *k* to *l*, and *l* to *m* were derived in a similar fashion. Equations 2, 4, 6, and 8 were used repeatedly to calculate the FE barriers and the equilibrated CA (ECA).

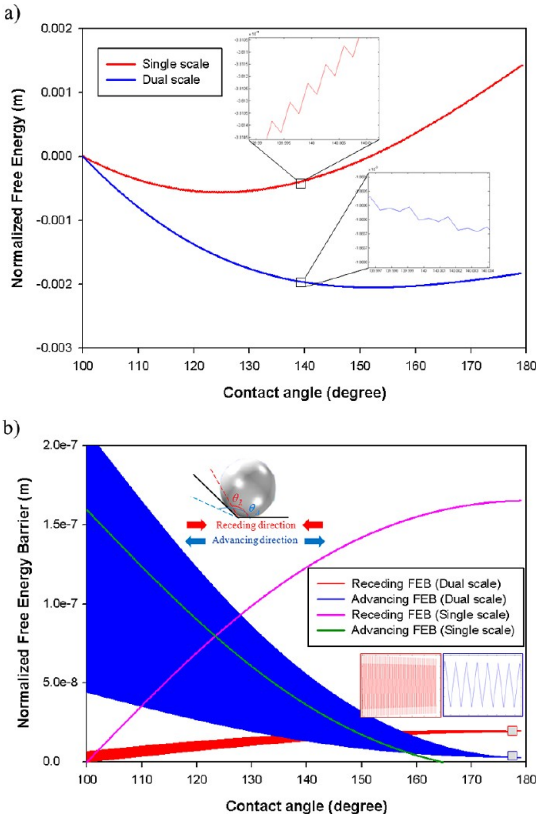

Figure 4. (a) Normalized free energy (FE) of the single-scale and dual-scale structures. The enlarged graphs show the variation in the local energy barriers indicating metastable and unstable regions. (b) Normalized receding and advancing free energy barriers (FEB) of the single-scale and dual-scale structures. The insets are the enlarged normalized free energy barriers (FEB).

From this, it is noticed that the dual-scale hierarchical structure has lower normalized free energy than the single-scale structure (Figure 4a). The single-scale structure has the fluctuated high free energy barrier (FEB), indicating that it is not easy to yield high CA (see the inset graph). On the other hand, the dual-scale structure shows the low FEB and the minimum FE is found at the CA over 150°, meaning high CA. The receding and advancing FEBs can give a complementary explanation on the results of the free energy of the single-scale and dual-scale structures (Figure 4b). The single-scale structure has monotonous variations in both of receding and advancing FEBs and the receding FEB rises rapidly. However, the dual-scale structure shows large fluctuations in both FEBs, and the receding FEB of the dual-scale structure is much smaller than that of the single-scale structure. Such a small receding FEB is the reason for the increase in the ECA of the dual-scale structure.

The synergistic interaction between nanoscale and microscale structures leads to an increase in the ECA. The multiscale hierarchical system can solely have superhydrophobic nature with a maximum ECA of 175° and a minimum ECA of 150° (Figure 5a). When the nanostructure is downsized, the resulting ECA is increased. Both of the nanostructure size and the pillar gap are important for obtaining high ECA. The existence of nanostructure is an indispensable requisite for high ECA. This theoretical interpretation will be helpful in designing superhydrophobic multiscale hierarchical surfaces in a more systematic manner.

Water Bouncing Effect. When a liquid droplet collides with a solid surface, it can exhibit bouncing, sticking, spreading, or pinning behaviors.[30] These behaviors vary according to the roughness and chemical composition of the solid surface and are also affected by such properties of the droplet as velocity, viscosity, and density.[31] For instance, depending on the droplet velocity, the behavior can be classified into three distinct regimes: nonbouncing regime due to low kinetic energy, bouncing regime following the Cassie−Baxter prediction, and sticky regime in which "touch-down" scenario may be achieved above a critical velocity.[32] Jung and Bhushan stated that the droplet velocity should be smaller than the critical velocity in order to develop a heterogeneous interface and water bouncing (*i.e.*, $V <$ func(γ_{LV}, H, $1/D$), where H is the pillar height, and D is the distance between pillars[21]). In all our experiments, each falling droplet had identical kinetic energy because the droplet velocity and droplet volume were fixed. Nevertheless, different dynamic behaviors were observed, including sticking phenomenon in the case of CNT and CNF forests and bouncing behavior over the CNT/ZnO and ZnO/CNF hybrid structures (Figure 5). Dimensionless numbers, *We* ($We = \rho RV^2/\gamma_{LV}$) and *Ca* ($Ca = \mu V/\gamma_{LV}$), have been employed by other researchers[23] to understand the correlation among the three regimes aforementioned. However, these numbers are not appropriate to describe different behavior in the regimes where identical dimensionless numbers are obtained due to the same droplet velocity V and liquid properties (ρ, γ_{LV}, μ); that is, no variation is expected in the dynamic behavior of the droplet. Therefore, effects of the different surface roughness structures on the liquid bouncing even with the same *We* and *Ca* values need to be explained through a new approach like numerical simulation. Such liquid bouncing takes place due to small dissipation of the kinetic energy of the droplet.[33] In this case, the kinetic energy can be transferred to the surface energy, and higher CA induces bouncing off like a solid springback.

The fundamental mechanism of liquid bouncing has yet to be fully understood because many factors are involved in it. In the present study, the threshold of FEB is adopted to explain the energy dissipation and surface energy conservation of a droplet on single-scale and multiscale nanostructures, and the resulting bouncing phenomenon due to the conserved surface energy is confirmed by the numerical analysis. The kinetic energy of a liquid droplet is converted into the

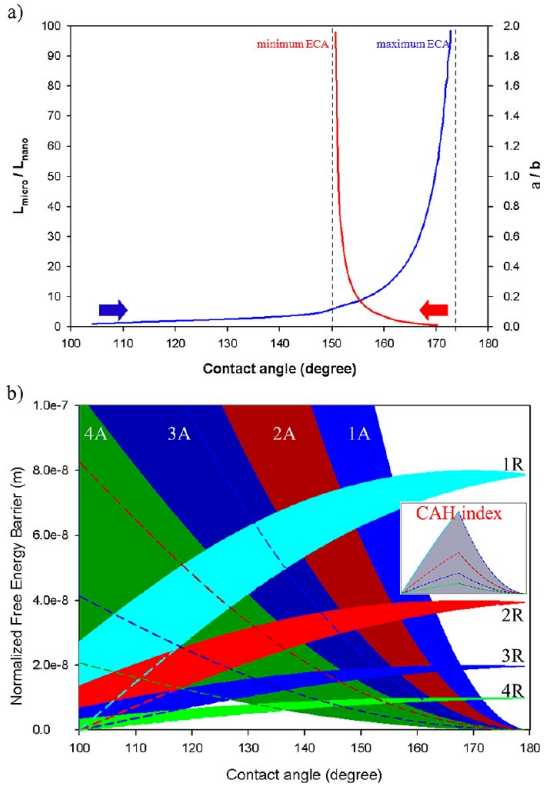

Figure 5. (a) Contact angle as a function of the ratio between micropillar size and nanopillar size and the density of nanopillars on the micropillar. The region between the two dashed lines represents ECAs obtainable in this system. (b) Normalized FEB as a function of system sizes; *a:b:d* = 80:200:1000 nm (1A and 1R), 40:100:500 nm (2A and 2R), 20:50:250 nm (3A and 3R), and 10:25:125 nm (4A and 4R). The shaded regions in the inset graph indicate the CAH index proposed in this study.

surface energy and dissipation energy when the liquid droplet bounces off the surface. The dissipation energy is determined by the surface geometry. For example, a low FEB can cause the dissipation energy of a droplet to decrease during deformation on the surface, and thus much of the kinetic energy is transferred into the surface energy. In this sense, the bouncing phenomenon on the multiscale hierarchical nanostructures can occur. On the other hand, the single-scale nanostructure has the similar advancing FEB but much higher receding FEB than the multiscale hierarchical nanostructure, which causes high energy dissipation and water sticking rather than bouncing (Figure 4b). This FEB characteristic can also be found as the entire system is downsized. Both the advancing FEB and receding FEB decrease with the system size (Figure 5b). The decrease in the FEB threshold makes it easier for a droplet to move toward advancing and receding directions, which decreases the energy dissipation significantly. In addition, CAH can be determined from the difference between the CAs of advancing FEB and receding FEB.[27] This is the maximum CAH where the vibrational energy of a system is ignored. However, since real systems possess nonzero vibrational energy during experiments, the presence of vibrational energy yields low CAH. Furthermore, now that the vibrational energy is not measurable, CAH cannot be determined quantitatively. Please note that the three intersecting curves, that is, the advancing FEB curve, receding FEB curve, and *x*-axis, form the shaded regions (see the inset graph). Here, we introduce a new physical parameter, "the CAH index" that indicates the area of the shaded region. The CAH index can help one understand the CAH characteristics of a complicated surface structure by providing more quantitative information, even in the case where vibrational energy is not known. The CAH and sliding angles of the dual-scale hierarchical nanostructures are lower than those of the single-scale nanostructures (Supporting Information, Figure 2). The results demonstrate that the surface morphology can also affect the dynamic motion of a liquid droplet. Additionally, a negligible difference was found in either the CAs or the CAHs measured between before and after the hydrophobic coating. This may be because the superhydrophobicity is determined mainly by the physical surface morphology but not by the chemical composition of the surface, especially in case of the Cassie (composite) state.[34]

The liquid droplet bouncing from the hierarchical surface was also demonstrated by FE simulation using the level set method. The simulation procedure was explained in detail in the Supporting Information. As illustrated by the experimental and simulation results, the liquid droplet with a CA of 120° does not bounce off, but it undergoes sticking and shaking motions (Figures 6a−c). When the CA is small enough, the energy dissipation due to the viscous nature of the liquid droplet becomes large and the energy transfer to the surface energy is minimized. Consequently, sticking occurs rather than bouncing off. On the contrary, the liquid droplet can bounce off as the CA increases since its kinetic energy is conserved by the surface deformation and not dissipated during the impact against the surface (Figures 6d−6f). These results are also consistent with the results of the thermodynamic analysis presented above.

Adhesion, which can explain the bouncing effect quantitatively, is expressed as follows:

$$W_{SL} = \gamma_{LV}(1 + \cos\theta) \quad (9)$$

where W_{SL} is the work of adhesion, and γ_{LV} is the surface tension of the liquid. The work of adhesion increases with decreasing CA. As a result, surfaces with low CA values have better wettability because more energy is dissipated from the inherent kinetic energy during colliding with the solid surface due to the liquid spreading.[31]

Overall, the bouncing phenomenon of a liquid droplet can occur when the following conditions are satisfied: (i) kinetic energy is transferred to surface energy,[35] (ii) inherent properties of the liquid droplet, *e.g.*, surface tension, viscosity, and density, are appropriate for the bounce-off regime in the *Ca* and *We*

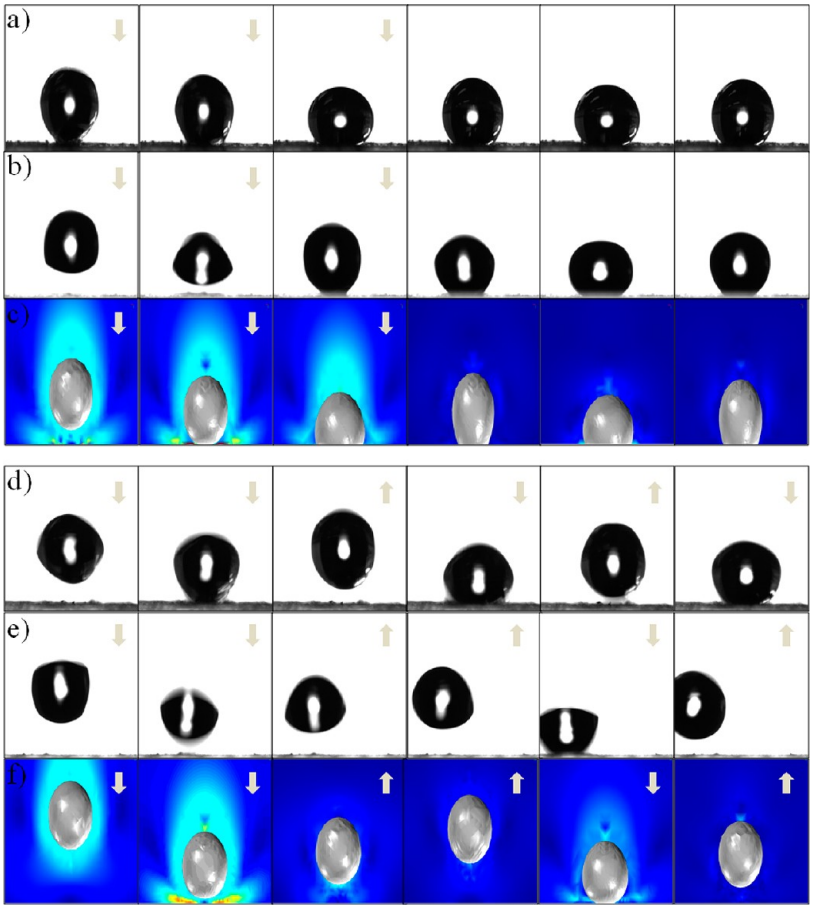

Figure 6. Experimental and simulation results of two distinct dynamic phenomena of a water droplet: (a) sticking of the droplet on the CNF forest, (b) sticking of the droplet on the CNT forest, (c) simulation results of the sticking droplet with a contact angle of 120°, (d) bouncing of the droplet over the ZnO/CNF multiscale hierarchical nanostructure, (e) bouncing of the droplet over the CNT/ZnO multiscale hierarchical nanostructure, and (f) simulation results of the bouncing droplet with a contact angle of 165°.

correlation,[23] and (iii) the kinetic energy dissipation is reduced by the superhydrophobic surface with hierarchical structures and stored in the surface deformation instead. A comprehensive understanding of such conditions is critical to materialize various applications such as liquid-repellent windshield, self-cleaning windows, exterior paint, and antifouling agents for roof tiles and textiles.

CONCLUSION

Single nanoscale structures, which show high hydrophobicity with a CA of 120−131°, were constructed with CNT forest, CNF forest, and ZnO pillars. To increase the CA further up to the level of superhydrophobicity, multiscale hierarchical structures were also prepared with CNT/ZnO and ZnO/CNF, and the resulting superhydrophobicity and dynamic effect (*i.e.*, bouncing effect) were analyzed. It was found that the multiscale hierarchical structures showed superhydrophobicity with CA values higher than 160° by means of the synergistic interaction of the first-level and the second-level hierarchical structures. The thermodynamic analysis accounted for the necessity of the multiscale hierarchical structures for superhydrophobicity. In contrast to the single-scale structures, the prepared multiscale hierarchical structures exhibited the bouncing phenomenon of a water droplet. To better understand such a phenomenon theoretically, FEB was analyzed and the FE simulation was carried out by using the level set method. As CA increases, the adhesion work, wettability, and energy dissipation of the droplet decrease. Consequently, the kinetic energy of the droplet can be converted into the surface deformation energy. Overall, the multiscale hierarchical structure is expected to serve as an indispensable platform to implement not only superhydrophobicity but also extreme water repellency.

METHODS

Fabrication of ZnO Pillars. ZnO nanorods were grown on p-type Si(100) substrates using the hydrothermal method.[36] The Si substrates were cleaned by soaking in the solution (H_2SO_4:H_2O_2 = 4:1) at 110 °C for 15 min and then in DI water for 5 min. ZnO seed nuclei for the growth of ZnO nanorods were prepared in 30 mM zinc acetate [$Zn(C_2H_3O_2)_2$] ethanol solution at 90 °C for 15 min. The solution was then spin coated onto the Si substrates at 1500 rpm for 60 s. Subsequently,

the seed-coated substrates were thermally annealed at 100 °C for 5 min for removal of the residual solvent. In this stage, the generated ZnO did not grow into the form of nanorods but it rather existed as a nucleus for growth of the ZnO nanorods. For the main growth, the Si substrates were immersed in an aqueous solution consisting of 25 mM zinc nitrate hexahydrate [$Zn(NO_3)_2 \cdot 6H_2O$], 25 mM hexamethylenetetramine [$C_6H_{12}N_4$] (HMT), and DI water. The main growth of the ZnO nanorods occurred at 90 °C for 60 min.

Fabrication of Multiscale CNT/ZnO and ZnO/CNF. Prepared CNF and CNT were used as a platform for the growth of ZnO nanorods. ZnO seed nuclei for ZnO nanorod growth were prepared in 30 mM zinc acetate [$Zn(C_2H_3O_2)_2$] ethanol solution at 90 °C for 15 min. The CNF and CNT were then immersed in the seed solution and the seed coated CNF and CNT were annealed at 300 °C for 5 min. After ZnO seed formation, ZnO nanorods were formed by the continuous supply of zinc ions and hydroxyl radicals in the aqueous solution consisting of 25 mM zinc nitrate hexahydrate [$Zn(NO_3)_2 \cdot 6H_2O$], 25 mM HMT, and DI water. The main growth of the ZnO nanorods was carried out at 90 °C for 30 min for CNF and 60 min for CNT. After the growth procedure, the aqueous solution including the grown ZnO nanorods was filtered using a microfilter paper (pore size, 1 μm). Finally, the CNF and CNT with ZnO nanorods were collected on the microfilter paper and dried at 40 °C for several hours in air.

Conflict of Interest: The authors declare no competing financial interest.

Acknowledgment. This study was supported by Basic Science Research Program through the National Research Foundation of Korea (NRF) funded by the Ministry of Education, Science and Technology (2010-0006337). Also, this study was supported by the Korea Science and Engineering Foundation (KOSEF) grant funded by the Korean government (MEST) (R11-2005-065) through the Intelligent Textile System Research Center (ITRC). The authors are grateful for the support.

Supporting Information Available: Fabrication of solvent etched CNT/polymer nanocomposites; contact angle (CA), contact angle hysteresis (CAH), and sliding angle (α) of the single-scale and dual-scale nanostructures before and after hydrophobic treatment; video clips of experimental and simulation results on the dynamic behavior of a water droplet over the single-scale surface and multiscale hierarchical surface; description of a numerical simulation procedure for a water droplet. This material is available free of charge *via* the Internet at http://pubs.acs.org.

REFERENCES AND NOTES

1. Marmur, A. Wetting on Hydrophobic Rough Surfaces: To Be Heterogeneous or Not To Be?. *Langmuir* **2003**, *19*, 8343–8348.
2. Li, H. J.; Wang, X. B.; Song, Y. L.; Liu, Y. Q.; Li, Q. S.; Jiang, L.; Zhu, D. B. Super-"Amphiphobic" Aligned Carbon Nanotube Films. *Angew. Chem. Int. Ed.* **2001**, *40*, 1743–1746.
3. Feng, L.; Li, S. H.; Li, H. J.; Zhai, J.; Song, Y. L.; Jiang, L.; Zhu, D. B. Super-Hydrophobic Surface of Aligned Polyacrylonitrile Nanofibers. *Angew. Chem. Int. Ed.* **2002**, *41*, 1221–1223.
4. Hosono, E.; Fujihara, S.; Honma, I.; Zhou, H. S. Superhydrophobic Perpendicular Nanopin Film by the Bottom-Up Process. *J. Am. Chem. Soc.* **2005**, *127*, 13458–13459.
5. Li, S. H.; Li, H. J.; Wang, X. B.; Song, Y. L.; Liu, Y. Q.; Jiang, L.; Zhu, D. B. Super-Hydrophobicity of Large-Area Honeycomb-like Aligned Carbon Nanotubes. *J. Phys. Chem. B* **2002**, *106*, 9274–9276.
6. Gleiche, M.; Chi, L. F.; Fuchs, H. Nanoscopic Channel Lattices with Controlled Anisotropic Wetting. *Nature* **2000**, *403*, 173–175.
7. Sun, M. H.; Luo, C. X.; Xu, L. P.; Ji, H.; Qi, O. Y.; Yu, D. P.; Chen, Y. Artificial Lotus Leaf by Nanocasting. *Langmuir* **2005**, *21*, 8978–8981.
8. Zhao, N.; Weng, L. H.; Zhang, X. Y.; Xie, Q. D.; Zhang, X. L.; Xu, J. A. Lotus-Leaf-like Superhydrophobic Surface Prepared by Solvent-Induced Crystallization. *Chemphyschem* **2006**, *7*, 824–827.
9. Zhai, L.; Cebeci, F. C.; Cohen, R. E.; Rubner, M. F. Stable Superhydrophobic Coatings from Polyelectrolyte Multilayers. *Nano Lett.* **2004**, *4*, 1349–1353.
10. Kim, H.; Noh, K.; Choi, C.; Khamwannah, J.; Villwock, D.; Jin, S. Extreme Superomniphobicity of Multiwalled 8 nnn TiO(2) Nanotubes. *Langmuir* **2011**, *27*, 10191–10196.
11. Jiang, L.; Zhao, Y.; Zhai, J. A Lotus-Leaf-like Superhydrophobic Surface: A Porous Microsphere/Nanofiber Composite Film Prepared by Electrohydrodynamics. *Angew. Chem. Int. Ed.* **2004**, *43*, 4338–4341.
12. Bhushan, B.; Jung, Y. C.; Niemietz, A.; Koch, K. Lotus-Like Biomimetic Hierarchical Structures Developed by the Self-Assembly of Tubular Plant Waxes. *Langmuir* **2009**, *25*, 1659–1666.
13. Bhushan, B.; Her, E. K. Fabrication of Superhydrophobic Surfaces with High and Low Adhesion Inspired from Rose Petal. *Langmuir* **2010**, *26*, 8207–8217.
14. Sharma, C. S.; Sharma, A.; Madou, M. Multiscale Carbon Structures Fabricated by Direct Micropatterning of Electrospun Mats of SU-8 Photoresist Nanofibers. *Langmuir* **2010**, *26*, 2218–2222.
15. Cui, Z.; Yin, L.; Wang, Q. J.; Ding, J. F.; Chen, Q. M. A Facile Dip-Coating Process for Preparing Highly Durable Superhydrophobic Surface with Multiscale Structures on Paint Films. *J. Colloid Interface Sci.* **2009**, *337*, 531–537.
16. Karunakaran, R. G.; Lu, C. H.; Zhang, Z. H.; Yang, S. Highly Transparent Superhydrophobic Surfaces from the Coassembly of Nanoparticles. *Langmuir* **2011**, *27*, 4594–4602.
17. Zhang, L.; Resasco, D. E. Single-Walled Carbon Nanotube Pillars: A Superhydrophobic Surface. *Langmuir* **2009**, *25*, 4792–4798.
18. Liu, H. H.; Zhang, H. Y.; Li, W. Thermodynamic Analysis on Wetting Behavior of Hierarchical Structured Superhydrophobic Surfaces. *Langmuir* **2011**, *27*, 6260–6267.
19. Nosonovsky, M. Multiscale Roughness and Stability of Superhydrophobic Biomimetic Interfaces. *Langmuir* **2007**, *23*, 3157–3161.
20. Nosonovsky, M.; Bhushan, B. Multiscale Effects and Capillary Interactions in Functional Biomimetic Surfaces for Energy Conversion and Green Engineering. *Philos Trans. R. Soc. A* **2009**, *367*, 1511–1539.
21. Jung, Y. C.; Bhushan, B. Dynamic Effects of Bouncing Water Droplets on Superhydrophobic Surfaces. *Langmuir* **2008**, *24*, 6262–6269.
22. Jung, Y. C.; Bhushan, B. Dynamic Effects Induced Transition of Droplets on Biomimetic Superhydrophobic Surfaces. *Langmuir* **2009**, *25*, 9208–9218.
23. Nosonovsky, M.; Bhushan, B. *Multiscale Dissipative Mechanisms and Hierarchical Surfaces*; Springer: 2008; p 172−175.
24. Feng, L.; Li, S. H.; Li, Y. S.; Li, H. J.; Zhang, L. J.; Zhai, J.; Song, Y. L.; Liu, B. Q.; Jiang, L.; Zhu, D. B. Super-Hydrophobic Surfaces: From Natural to Artificial. *Adv. Mater.* **2002**, *14*, 1857–1860.
25. Luo, C.; Zuo, X. L.; Wang, L.; Wang, E. G.; Song, S. P.; Wang, J.; Wang, J.; Fan, C. H.; Cao, Y. Flexible Carbon Nanotube-Polymer Composite Films with High Conductivity and Superhydrophobicity Made by Solution Process. *Nano Lett.* **2008**, *8*, 4454–4458.
26. Jeong, H. E.; Lee, S. H.; Kim, J. K.; Suh, K. Y. Nanoengineered Multiscale Hierarchical Structures with Tailored Wetting Properties. *Langmuir* **2006**, *22*, 1640–1645.
27. Li, W.; Amirfazli, A. A Thermodynamic Approach for Determining the Contact Angle Hysteresis for Superhydrophobic Surfaces. *J. Colloid Interface Sci.* **2005**, *292*, 195–201.
28. Wang, S. R.; Zhang, Y.; Abidi, N.; Cabrales, L. Wettability and Surface Free Energy of Graphene Films. *Langmuir* **2009**, *25*, 11078–11081.
29. Han, J.; Gao, W. Surface Wettability of Nanostructured Zinc Oxide Films. *J. Electron. Mater.* **2009**, *38*, 601–608.
30. Reyssat, M.; Pepin, A.; Marty, F.; Chen, Y.; Quere, D. Bouncing Transitions on Microtextured Materials. *Europhys. Lett.* **2006**, *74*, 306–312.

31. Okumura, K.; Chevy, F.; Richard, D.; Quere, D.; Clanet, C. Water Spring: A Model for Bouncing Drops. *Europhys. Lett.* **2003**, *62*, 237–243.
32. Bartolo, D.; Bouamrirene, F.; Verneuil, E.; Buguin, A.; Silberzan, P.; Moulinet, S. Bouncing or Sticky Droplets: Impalement Transitions on Superhydrophobic Micropatterned Surfaces. *Europhys. Lett.* **2006**, *74*, 299–305.
33. Richard, D.; Quere, D. Bouncing Water Drops. *Europhys. Lett.* **2000**, *50*, 769–775.
34. Lee, D. J.; Cho, K. Y.; Jang, S.; Song, Y. S.; Youn, J. R. Liquid Slip on a Nanostructured Surface. *Langmuir* **2012**, *28*, 10488–10494.
35. Callies, M.; Quere, D. On Water Repellency. *Soft Matter* **2005**, *1*, 55–61.
36. Vayssieres, L. Growth of Arrayed Nanorods and Nanowires of ZnO from Aqueous Solutions. *Adv. Mater.* **2003**, *15*, 464–466.